analytical chemistry

Article

pubs.acs.org/ac

Real-Time Imaging of Mitochondrial Hydrogen Peroxide and pH Fluctuations in Living Cells Using a Fluorescent Nanosensor

Limin Yang,[†] Na Li,[†] Wei Pan, Zhengze Yu, and Bo Tang*

College of Chemistry, Chemical Engineering and Materials Science, Collaborative Innovation Center of Functionalized Probes for Chemical Imaging in Universities of Shandong, Key Laboratory of Molecular and Nano Probes, Ministry of Education, Shandong Provincial Key Laboratory of Clean Production of Fine Chemicals, Shandong Normal University, Jinan 250014, P. R. China

Supporting Information

ABSTRACT: Mitochondrial reactive oxygen species (ROS) and pH fluctuations are closely correlated with mitochondrial dysfunctions, which are implicated in various human diseases including neurodegenerative disorders and cancers. Simultaneously monitoring the changes of ROS and pH of mitochondria remains a major challenge in the mitochondrial biology. In this study, we develop a novel mitochondria-targeted fluorescent nanosensor for real-time imaging of the fluctuations of hydrogen peroxide (H_2O_2) and pH in living cells. The fluorescence probes for detecting pH and H_2O_2 were loaded in the small-sized mesoporous silica nanoparticles (MSN). Then the polyethylenimine was attached to cap the pores of MSN, the triphenylphosphonium was further modified to target mitochondria in living cells. Confocal fluorescence imaging indicated that the nanosensor could effectively target mitochondria and successfully achieved real-time imaging of mitochondrial H_2O_2 and pH fluctuations in living cells. Notably, this is a single nanosensing system that is capable of visualizing multiple subcellular analytes at the same time and position by multicolor fluorescence imaging. The current approach can provide a promising tool to investigate the interplaying roles of various subcellular analytes in living cells.

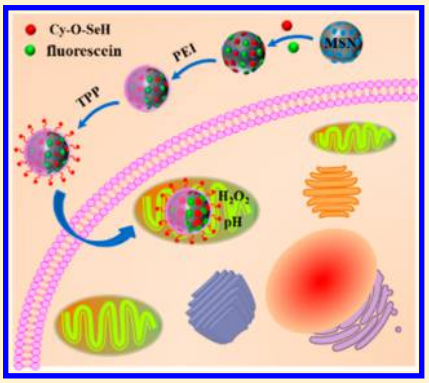

Mitochondria undertake multiple critical functions, such as generating adenosine triphosphate and initiating cellular apoptosis.[1−3] Mitochondrial dysfunction is involved in various human diseases, including obesity, diabetes, neurodegenerative disorders, and cancers.[4−7] A major cause of damage for many of these diseases is the overproduction of reactive oxygen species (ROS) in mitochondria.[8,9] In particular, with hydrogen peroxide (H_2O_2) as a prominent member of the ROS family,[10] aberrant production or accumulation of H_2O_2 within mitochondria is frequently implicated in mitochondrial dysfunction.[11] Moreover, the fluctuation of H_2O_2 usually follows with the alterations of membrane potential or pH in mitochondria,[12−14] leading to inevitable influence of mitochondrial physiological function. In the process of inducing cell apoptosis, the individual or simultaneous changes of H_2O_2 and pH are commonly accompanied.[15−18] In view of the interplaying roles of H_2O_2 and pH in cell apoptosis and disease, real-time monitoring the variations of H_2O_2 and pH in mitochondria of living cells is therefore crucial to the understanding of mitochondrial physiology and pathology.

Many molecular fluorescent probes and green fluorescent protein probes have been designed and synthesized for detecting and imaging mitochondrial H_2O_2[12,19−22] or pH[23−26] in living cells. As these fluorescent probes are specific to H_2O_2 or pH, they are not able to simultaneously respond to H_2O_2 and pH in mitochondria. A potential solution for the problem is to employ two fluorescent probes in a cell. However, it is difficult to detect multiple analytes at the same position in mitochondria when utilizing several different fluorescent probes. To achieve the real-time monitoring of mitochondrial H_2O_2 and pH changes, some prerequisites should be met: (a) the probe should be specific mitochondria-targeting, (b) it should have a reversible H_2O_2-dependent and pH-dependent sensing without mutual interference, and (c) it should possess different emission profiles to avoid the spectral overlap and selectively discriminate the changes between H_2O_2 and pH. Thus, it is an unprecedented challenge for simultaneously monitoring the changes of H_2O_2 and pH in mitochondria using a single fluorescent probe.

Herein, we develop a novel fluorescent nanosensor for real-time detecting and imaging of the mitochondrial H_2O_2 and pH fluctuations in living cells. Mesoporous silica nanoparticles (MSN) were selected as the carrier due to their good biocompatibility, high loading capacity, and easy functionalization.[27−29] The molecular fluorescence probes, Cy-O-SeH[21] for H_2O_2 and fluorescein for pH, were employed to detect the changes of H_2O_2 and pH, respectively. After these probes were loaded in the pores of MSN, the polyethylenimine (PEI) was attached to the surface of the MSN via electrostatic interaction for blocking the pores. Further conjugation of the triphenylphosphonium (TPP) moiety by amide bonds endows the nanosensor with specific mitochondria targeting. The designed nanosensor is capable of real-time monitoring the changes of

Received: October 24, 2014
Accepted: March 4, 2015
Published: March 4, 2015

DOI: 10.1021/ac503975x
Anal. Chem. 2015, 87, 3678−3684

pH and H_2O_2 in mitochondria of living cells by bicolor imaging. The details of this strategy are displayed in Scheme 1.

Scheme 1. Illustration of the Nanosensor for Imaging of Mitochondrial H_2O_2 and pH

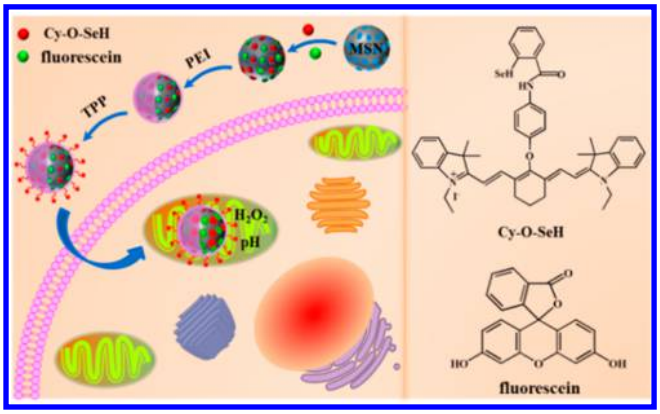

EXPERIMENTAL SECTION

Materials. Tetraethyl orthosilicate (TEOS), hexadecyl trimethylammonium chloride (CTAC), triethanolamine (TEA), fluorescein, and ethanol were obtained from China National Pharmaceutical Group Corp. (Shanghai, China). Nigericin was obtained from APOLLO Scientific Ltd. (4-carboxybutyl)triphenylphosphonium bromide and polyethylenimine (M.W. 10000) were obtained from Alfa Aesar Chemical Ltd. (Tianjin, China). Mito-Tracker Green and Lyso-Tracker Green were purchased from Molecular Probes (Invitrogen, USA). Dichloroacetate was purchased from Adamas Reagent Ltd. (Shanghai, China). 2-(N-Morpholino)ethanesulfonic acid (MES), 4-(2-hydroxyethyl)-1-piperazineethanesulfonic acid (HEPES), 1-ethyl-3-(3-dimethly aminopropyl) carbodiimide (EDC), and 3-(4,5-dimethylthiazol-2-yl)-2,5-diphenyltetrazolium bromide (MTT) were obtained from Sigma-Aldrich. The human breast cancer cell line MCF-7 was purchased from KeyGEN biotechnology Company (Nanjing, China), and the normal immortalized human mammary epithelial cell line MCF-10A was purchased from Shanghai Bioleaf Biotechnology Company (Shanghai, China). Human cervical cancer cell line Hela was purchased from Committee on Type Culture Collection of the Chinese Academy of Sciences. All the chemicals were analytical grade and used without further purification. Water was purified with a Sartorius Arium 611 VF system (Sartorius AG, Germany) to a resistivity of 18.2 MΩ·cm. Cy-O-SeH was synthesized according to our previous report.[21] Cy-O-SeH was obtained by the reaction of Cy-O-Eb with glutathione. ^{1}H NMR, ^{13}C NMR, ^{77}Se-NMR, and MS were employed to characterize Cy-O-Eb. ^{1}H NMR (300 MHz, DMSO-d_6, 25 °C, TMS): δ 8.11 (d, J = 9.0 Hz, 1H), 7.84 (d, J = 13.5 Hz, 2H), 7.62 (d, J = 9.0 Hz, 3H), 7.52−7.45 (m, 4H), 7.36 (m, 4H), 7.25−7.19 (m, 4H), 6.20 (d, J = 13.5 Hz, 2H), 4.17 (4H), 2.75 (4H), 1.94 (2H), 1.32 (s, 12H), 1.27−1.22 (t, J = 6.9 Hz, 6H). ^{13}C NMR (300 MHz, CD_3COCD_3, 25 °C): δ 1171.8, 165.8, 162.6, 157.8, 141.6, 141.2, 138.3, 134.4, 133.3, 132.2, 130.9, 129.5, 128.7, 128.6, 128.3, 128.1, 127.9, 127.4, 126.2, 125.8, 125.2, 124.3, 122.5, 115.4, 115.0, 110.3, 99.5, 65.6, 60.4, 49.2, 39.7, 36.6, 31.9, 31.5, 30.6, 29.7, 29.3, 28.0, 27.2, 26.8, 25.6, 24.7, 22.7, 21.2, 20.4, 19.2. ^{77}Se-NMR (300 MHz, CD_3COCD_3, 25 °C): δ 457.46. MS calculated for [M$^+$]: 766.2906. Found: 766.2805. One peak at m/z 768.307 is corresponding to the protonated selenol free radical.

Instruments. High resolution transmission electron microscopy (HRTEM) was carried out on a JEM-2100 electron microscope. NMR spectra were taken on a nuclear magnetic resonance spectrometer (AVANCE 300, Bruker, Switzerland). Molecular weight was acquired from an UPLC-LTQ orbitrap mass spectrometer (Thermo Fisher Scientfic, San Jose, CA). Fluorescence spectra were obtained with an FLS-920 Edinburgh Fluorescence Spectrometer with a xenon lamp. All pH measurements were performed with a pH-3c digital pH-meter (Shanghai LeiCi Device Works, Shanghai, China) with a combined glass-calomel electrode. Absorbance was measured in a microplate reader (Synergy 2, Biotek, USA) in the MTT assay. Success of each reaction step was confirmed by monitoring the changes in zeta potential with a Malvern Zeta Sizer Nano (Malvern Instruments). Confocal fluorescence imaging was performed with a TCS SP5 confocal laser scanning microscope (Leica Co., Ltd. Germany).

Preparation of Mesoporous Silica Nanoparticles (MSN). MSN was typically synthesized according to a reported protocol with some modifications.[30] A total of 0.5 g of CTAC was dissolved in 20 mL of water followed by the addition of TEA (80 mg). The mixture was heated at 95 °C under intensive stirring for 1 h. Then, 1.5 mL of TEOS was added dropwise under stirring for another 1 h. The as-synthesized MSN was washed with methanol several times to remove the residual reactants. The collected products were calcined at 450 °C for 10 h to remove the CTAC remaining inside the mesopores absolutely.

Assembly of the Nanosensor. A total of 2.0 mg of MSN was added and dispersed in 1.0 mL of fluorescein and Cy-O-SeH solution (0.1 mg/mL). The mixture was stirred for 12 h in darkness. Then, the above solution was centrifuged (12 000 rpm, 10 min) to remove the molecules absorbed physically on the outer surface of the MSN. The precipitates were dispersed in 1 mL of PEI solution with gentle stirring for 12 h in darkness. To optimize the PEI amount for the nanosensor, the as-prepared 1 mL nanosensor (0.1 mg/mL) solution with different amounts of PEI was stored at room temperature and the fluorescence intensity of the sample was measured at 0 and 24 h. As shown in Figure S1, the nanosensor with low amonts of PEI would lead to obvious leakage of Cy-O-SeH and fluorescein. The leakage amount of fluorescein and Cy-O-SeH decreased with the increase amount of PEI. When the concnetration of PEI reached 0.2 mg/mL, the leakage amount was not changed any more. Therefore, 0.2 mg/mL of PEI was applied in this study. After that, the precipitates were centrifuged (12 000 rpm, 10 min) and dispersed in the 10.0 mM MES (pH = 6.0). The nanosensor was obtained by coupling the carboxyl group of the TPP and the amino group on the surface of PEI to form the amido bond. EDC solution (1.5 mM) was added to TPP (0.5 mM) solution, and the solution was mixed and reacted for 30 min at room temperature to activate carboxylate groups. The mixture solution was reacted for 24 h with gentle stirring in darkness, which resulted in the formation of the amido bond. The resulting precipitates were centrifuged (12 000 rpm, 10 min) and washed three times with water.

Quantitation of Fluorescein, Cy-O-SeH, and TPP Loaded on the Nanosensor. A total of 1 mL of nanosensor (0.1 mg/mL) solution was heated in the water bath at 70 °C for 1 h. The sample was centrifuged (12 000 rpm, 10 min), and the

DOI: 10.1021/ac503975x
Anal. Chem. 2015, 87, 3678−3684

supernate was separated. Then, the precipitates were redispersed in 1 mL of HEPES buffer. The above procedure was repeated to ensure the complete release of fluorescein and Cy-O-SeH from the pores. The fluorescence intensity of the supernate was measured, and the concentrations of fluorescein and Cy-O-SeH were determined according to the standard linear calibration curve of fluorescein and Cy-O-SeH, respectively.

To quantify the modified amount of TPP on the nanosensor, an MSN-PEI-TPP nanocomposite (MSN-PT) was prepared. After MSN-PEI reacted with TPP, the sample solution was centrifuged and the supernate was separated. Then, the precipitates were redispersed and further centrifuged to ensure the complete release of the adsorbed TPP from MSN. According to the standard linear calibration curve of TPP, the concentration of TPP on the nanosensor was obtained by subtracting the concentration of TPP in the supernatant from the total concentration of TPP added into the reaction solution.

General Procedure for Fluorescence Determination. A series of standard pH buffers of 10 mM HEPES were prepared. The fluorescence spectra of nanosensor solution (0.1 mg/mL) with different standard pH's was collected with λex/λem = 488/512 nm.

For the detection of H_2O_2, different concentrations of H_2O_2 were added to the nanosensor solution (0.1 mg/mL). The mixture was equilibrated and laid aside at 37 °C for 30 min before determination. The fluorescence of the samples was measured at λex/λem = 768/780 nm.

To investigate the selectivity of the nanosensor toward H^+, metal ions (Cu^{2+}, Fe^{3+}, Co^{2+}, Fe^{2+}, Mg^{2+}, Na^+, Zn^{2+}, Mn^{2+}, K^+, Ca^{2+}) as well as oxidative-stress-associated redox chemicals, including glutathione (GSH) and H_2O_2, were examined. All data were obtained using an excitation wavelength at 488 nm. Effects of pH on fluorescence intensities of the nanosensor toward H_2O_2 in HEPES buffer (10 mM) were also tested. The concentration of H_2O_2 is 200 μM. All data were obtained using an excitation wavelength at 768 nm.

The pH of the nanosensor between pH 5 and pH 9 was adjusted back and forth by 2.5 M HCl or NaOH, and then measured with a pH meter. The fluorescence spectra were recorded with λex = 488 nm. Redox cycling of the nanosensor was done by the addition of 100 μM H_2O_2 and 400 μM GSH in 10 mM HEPES with pH = 7.4. The fluorescence spectra were recorded with λex = 768 nm.

Cell Culture. MCF-7, Hela, and MCF-10A cells were cultured in Dulbecco's modified Eagles medium (DMEM) with 10% fetal bovine serum and 100 U/mL of 1% antibiotics penicillin/streptomycin and maintained at 37 °C in a 100% humidified atmosphere containing 5% CO_2.

MTT Assay. MCF-7 cells were cultured in 96-well microtiter plates and incubated at 37 °C in 5% CO_2 for 24 h. After the original medium was removed, the cells were incubated with the nanosensor (0.05, 0.1, 0.2 mg/mL) for 6, 12 and 24 h, respectively. Next, 150 μL of MTT solution (0.5 mg/mL) was added to each well. After 4 h, the remaining MTT solution was removed, and 150 μL of DMSO was added to each well to dissolve the formazan crystals. The absorbance was measured at 490 nm with the RT 6000 microplate reader. The experiment was repeated three times, and the data are shown as the mean ± SD.

Confocal Fluorescence Image Assay. Cells were plated on chamber slides for 24 h. Then, the nanosensor (0.1 mg/mL) was delivered into the cells in DMEM for 6 h at 37 °C in 5% CO_2. Then, cells were washed three times with PBS buffer to remove the nanosensor that were not taken up into the cells. The cells were examined by confocal laser scanning microscopy (CLSM) with different laser transmitters. All experimental parameters (the laser intensity, exposure time, objective lens) were stationary when the different fluorescence images were captured. The fluorescence intensity (FI) was the average fluorescence intensity of the cell area (at least 50 cells) from the confocal fluorescence images, which was quantified by LAS AF software.

In colocalization imaging experiments, MCF-7 cells were incubated with 0.1 mg/mL of MSN-Cy-O-SeH-PEI (MSN-CP) or MSN-Cy-O-SeH-PEI-TPP (MSN-CPT) for 6 h, washed three times with PBS (pH 7.4), and then incubated with Mito-Tracker Green (MTG, 25 nM) for 15 min. Before fluorescence imaging, the adherent cells were further washed with PBS (pH 7.4) three times to remove the excess MTG. Confocal fluorescence imaging of MTG-stained cells were captured using a 488 nm laser; the collection window is 500−580 nm. The excitation wavelength of MSN-CP or MSN-CPT is 633 nm, and the collection window is 700−800 nm.

The MCF-7 cells treated with the nanosensor (0.1 mg/mL) for 6 h at 4 and 37 °C were investigated. To study the intracellular delivery pathway of the nanosensor, Hela cells were incubated with 0.1 mg/mL of MSN-CPT various times, washed with PBS (pH 7.4), and then incubated with Mito-Tracker Green (MTG, 25 nM) or Lyso-Tracker Green (LTG, 100 nM) for 15 min, respectively. Before fluorescence imaging, the adherent cells were further washed with PBS (pH 7.4) three times to remove the excess MTG or LTG. The excitation wavelength of MTG or LTG is 488 nm, the collection window is 500−580 nm. The excitation wavelength of MSN-CPT is 633 nm, and the collection window is 700−800 nm.

To assess the applicability of the nanosensor to intracellular pH response, the nanosensor-loaded MCF-7 cells were incubated at 37 °C for 15 min in a high K^+ buffer (120 mM KCl, 1 mM $CaCl_2$, 0.5 mM $MgSO_4$, 30 mM NaCl, 1 mM NaH_2PO_4, 5 mM glucose, and 20 mM HEPES) at various pH values (5.3−8.2) in the presence of 10.0 μM nigericin. After 20 min, cell imaging was carried out after washing cells with PBS (pH 7.4) three times. The image was obtained by using excitation at 488 nm and an emission filter at 500−580 nm in the green channel.

To demonstrate the applicability of the nanosensor to sensing intracellular H_2O_2, different concentrations of H_2O_2 were added into the nanosensor-loaded MCF-7 cells for 20 min. Cell imaging was carried out after washing the cells with PBS (pH 7.4) three times. The image was obtained by using excitation at 633 nm and an emission filter at 700−800 nm in the red channel.

The experiments were further performed to evaluate the availability of the nanosensor for monitoring the changes of H_2O_2 and pH in MCF-7 and MCF-10A cells by dichloroacetate (DCA) stimulus. The nanosensor-loaded cells were stimulated by 1.0 mM DCA. Alternatively, the nanosensor-treated cells were coincubated with DCA (1.0 mM) and rotenone (10.0 μM). MCF-7 cells treatments with the nanosensor in the presence of DCA under different times were performed. Prior to imaging, cell imaging was carried out after washing cells with PBS three times. In the green channel, the image for fluorescein was obtained by using excitation at 488 nm and an emission filter at 500−580 nm. In the red channel, the image for Cy-O-

DOI: 10.1021/ac503975x
Anal. Chem. 2015, 87, 3678−3684

SeH was obtained by using excitation at 633 nm and an emission filter at 700−800 nm.

To study the changes of the mitochondrial membrane potential of cells in the presence of 100 μM H_2O_2 or 1.0 mM DCA, cells were then incubated with rhodamine 123 (5 μg/mL) for 15 min in darkness at 37 °C. After loading, cells were washed three times with PBS. Confocal fluorescence imaging of rhodamine 123-stained cells was obtained by excitation of the samples at 488 nm and an emission filter at 500−580 nm in the green channel.

RESULTS AND DISCUSSION

Preparation and Characterization of the Nanosensor. The MSNs were typically synthesized according to a reported protocol with some modifications.[30] As shown in Figure 1, the

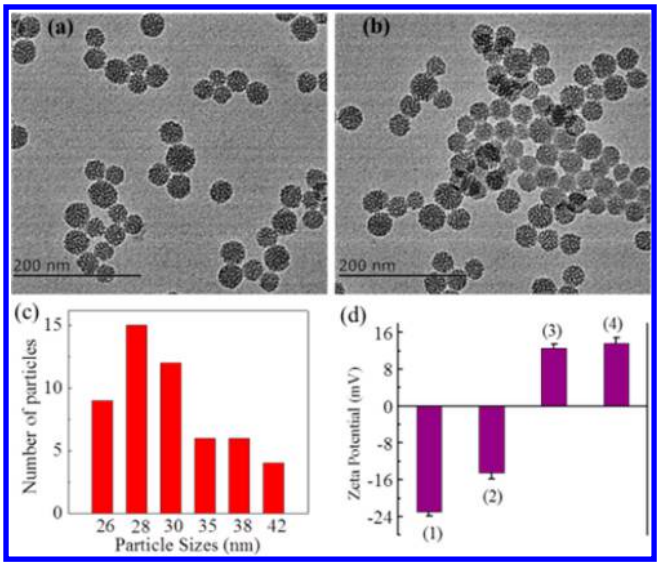

Figure 1. TEM image of MSN (a) and nanosensor (b). (c) Size distribution of the prepared MSN. (d) Zeta potential of the every step modification: (1) MSN, (2) MSN-fluorescein-Cy-O-SeH, (3) MSN-fluorescein-Cy-O-SeH-PEI, (4) nanosensor.

size of MSN was about 30 nm (Figure 1a,c). The morphology of the nanosensor did not show obvious change compared with MSN (Figure 1b). Furthermore, a zeta potential experiment was employed to confirm the assembly process of every step for the nanosensor (Figure 1d). The zeta potential of the as-synthesized MSN was −22.9 ± 1.2 mV. After loading the fluorescein and Cy-O-SeH, the zeta potential was changed to −14.5 ± 1.6 mV. With further modification of PEI and TPP, the zeta potentials were +12.6 ± 1.15 and +13.6 ± 1.31 mV, respectively. The results confirmed that the nanosensor was successfully assembled. The amounts of loaded fluorescein and Cy-O-SeH in the nanosensor were calculated to be 1.3 mg/g and 8.2 mg/g, respectively (Figure S2). The content for the targeting ligand (TPP) was determined to be 5.6 mg per 1 g of nanosensor (Figure S3). Moreover, the encapsulation of the fluorescein and Cy-O-SeH in MSN barely influence its properties for detection of pH and H_2O_2, respectively (Figure S4).

The Responses of Nanosensor Toward to H_2O_2 and pH. The fluorescence responses of the nanosensor for different pH values are shown in Figure 2a. With the increase of pH values, the fluorescence intensity of the nanosensor at 512 nm increased gradually. There was a good linearity between

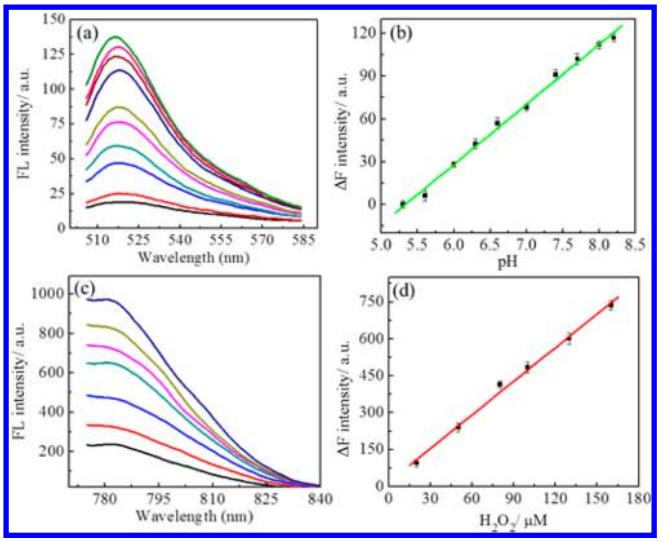

Figure 2. (a) Fluorescence spectra of the nanosensor with various pH values from 5.3 to 8.2 (λex = 488 nm, 10 mM HEPES). (b) Linear fitting of the pH-dependent fluorescence intensity at 512 nm. ($\Delta F = F - F_{5.3}$). (c) Fluorescence spectra of the nanosensor with various concentrations of H_2O_2 (λex = 768 nm, 10 mM HEPES, pH = 7.4). (d) Linear fitting of the H_2O_2-dependent fluorescence intensity at 780 nm ($\Delta F = F - F_0$, F_0 is the fluorescence intensity of the nanosensor without H_2O_2).

fluorescence intensity and pH in the range from 5.3 to 8.2 (Figure 2b), which covers most of the physiological pH ranges. Therefore, it suggested that the nanosensor could be used to monitor the mitochondrial pH changes due to its wide linear range. To investigate the selectivity of the nanosensor toward H^+, metal ions (Na^+, K^+, Mg^{2+}, etc.) and oxidative-stress-associated redox chemicals, including glutathione (GSH) and H_2O_2, were examined in parallel under the same conditions. As shown in Figure S5, the nanosensor showed an excellent selectivity response to H^+ under these conditions, indicating that the nanosensor could be used to monitor mitochondrial pH without interference.

Next, the response of the nanosensor toward H_2O_2 was investigated. The fluorescence intensity of the nanosensor was recorded under various concentrations of H_2O_2. As shown in Figure 2d, there was a good linearity between relative fluorescence intensity at 780 nm and concentrations of H_2O_2 from 20 to 160 μM. Moreover, the fluorescent signals did not obviously change in different pH (Figure S6). It demonstrated that the designed nanosensor was able to individually or simultaneously monitor H_2O_2 and pH fluctuations without mutual interference.

The experiment was further performed to study the reversibility of the nanosensor. As shown in Figure 3a, the nanosensor reveals an excellent reversibility between pH 5 and pH 9. The reversible oxidation−reduction cycles of the nanosensor were mediated by H_2O_2 or GSH. It displays that the reversible oxidation−reduction cycle could be repeated two times with only a modest fluorescence decrement (Figure 3b). These results indicate that the nanosensor is suitable for real-time monitoring the redox state and pH changes.

MTT Assay. To evaluate the cytotoxicity of the nanosensor, we performed an MTT assay in the human breast cancer cell line (MCF-7). The absorbance of MTT at 490 nm depends on the degree of activation of the cells. The cell viability was expressed by the ratio of the absorbance of the treated cells

DOI: 10.1021/ac503975x
Anal. Chem. 2015, 87, 3678−3684

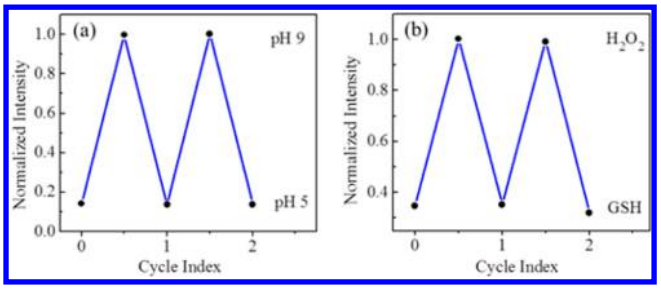

Figure 3. (a) pH reversibility study of the nanosensor between pH 5 and 9 in HEPES buffer (10 mM). (b) Redox reversibility study of the nanosensor between H_2O_2 and GSH in HEPES buffer (10 mM, pH = 7.4). (a) λex/λem = 488/512 nm, (b) λex/λem = 768/780 nm.

(incubated with the nanosensor) to that of the untreated cells. Figure S7 showed that the cell viability was more than 90% with different incubation time and concentrations, suggesting that the nanosensor exhibited almost no cytotoxicity or side effects in living cells. It indicated that the nanosensor was an approving candidate when applied in living cells.

Co-staining Imaging in Living Cells. We next performed colocalization imaging experiments in MCF-7 cells to assess whether the nanosensor could selectively locate in mitochondria. Mito-Tracker Green (MTG), a commercial mitochondrial dye, was chosen to label mitochondria. The excitation and emission spectra of MTG and fluorescein are overlapped. To avoid the interference from fluorescein, only Cy-O-SeH was loaded in the MSN. MSN-Cy-O-SeH-PEI-TPP nanocomposite (MSN-CPT) was prepared after PEI and TPP modified on the surface of MSN. The MSN-Cy-O-SeH-PEI nanocomposite (MSN-CP) without TPP was also synthesized. After MCF-7 cells incubated with MSN-CPT or MSN-CP, the cells were additionally stained with MTG to label mitochondria. As can be seen from Figure 4A(c), a well overlapped imaging (Pearson's correlation coefficient, ρ = 0.65) was obtained for MSN-CPT as evidenced by the clear yellow signals. It confirmed that the MSN-CPT could specifically localize in mitochondria of living cells. In contrast, the MSN-CP randomly distributed inside the

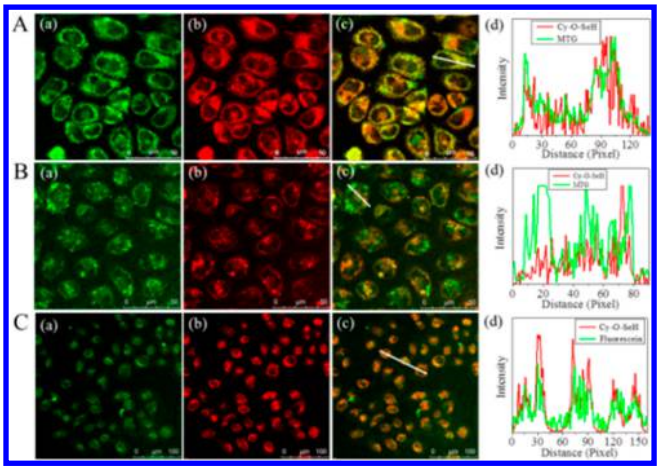

Figure 4. Confocal fluorescence image of MCF-7 cells treated with MSN-CPT (A), MSN-CP (B), and nanosensor (C). (A and B) Green channel for MTG and the red channel for Cy-O-SeH, respectively. (C) Green channel for fluorescein and the red channel for Cy-O-SeH. (c) Overlay image of a and b. (d) Fluorescence intensity profile of regions of interest (white line in c) across the lines. Green channels and red channels are excitated at 488 and 633 nm, respectively.

cells without specific mitochondrial localization (Pearson's correlation coefficient, ρ = 0.26) under the same conditions (Figure 4B(c)). A certain degree of mitochondrial localization was observed for MSN-CP, which contributes to the positive charge on the surface of MSN-CP. It suggested that an appropriate targeting ligand TPP on the surface of the nanosensor was an indispensable part for realizing mitochondria targeting. Further experimentation shows a good overlay image of fluorescein and Cy-O-SeH of the nanosensor (Figure 4C(c)), implying that the nanosensors possess the ability to detect analytes at the same position of mitochondria in living cells. The above observations are further verified by quantifying the line scanning profiles of fluorescent intensity.

Intracellular Delivery Pathway of the Nanosensor. The interaction of the cells with the nanosensor at 4 and 37 °C was first investigated. As shown in Figure S8, the intracellular fluorescence was obviously decreased at 4 °C, which demonstrated that the nanosensor was internalized by cells via an energy-dependent endocytosis process. Further experiments showed that the intracellular delivery pathway of the nanosensor was from lysosome to mitochondria by the time-dependent uptake study (Figures S9, S10). The lysosomes' delivery pathway of the nanoparticles sometimes influences the specificity of its mitochondria targeting.[31]

Imaging the H_2O_2 and pH Fluctuations in Mitochondria of Living Cells. To verify the dynamic imaging features, the nanosensor was used to monitor pH and H_2O_2 changes in living cells. First, we investigate the response of nanosensor treated MCF-7 cells under different pH values. The intracellular pH was homogenized with the high K^+ buffer and ionophore nigericin.[32] The fluorescence intensity of the fluorescein inside cells enhances gradually with the increase of pH values in the green channel (Figure 5A, Figure S11) under confocal laser

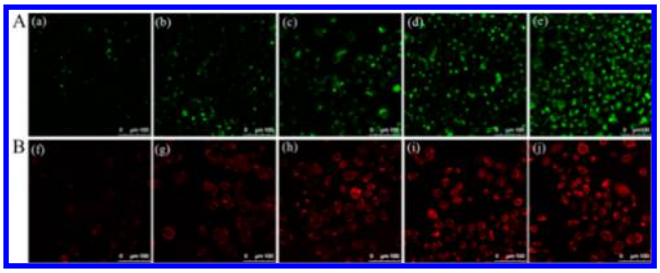

Figure 5. (A) Confocal fluorescence imaging of MCF-7 cells treated with the nanosensor at pH 5.3−8.2 (a−e). (B) Confocal fluorescence imaging of MCF-7 cells treated with the nanosensor at different concentrations of H_2O_2 (0−150 μM, f−j). The excitation wavelength of A is 488 nm. The excitation wavelength of B is 633 nm. Scale bars are 100 μm.

scanning microscopy (CLSM). It indicated that the nanosensor was able to monitor and image mitochondrial pH fluctuations in living cells. Then the fluorescence response of nanosensor treated cells in the presence of H_2O_2 was carried out. As shown in Figure 5B, the red fluorescence signal in cells increased successively with the increase of H_2O_2 concentrations (Figure S12), implying that the nanosensor is capable of imaging the changes in the level of H_2O_2 within mitochondria. Thus, the overall results reveal that the developed nanosensor can be utilized for monitoring and imaging mitochondrial pH and H_2O_2 fluctuations in living cells.

Interestingly, an increased red fluorescence was observed while the green fluorescence intensity was decreased in the

DOI: 10.1021/ac503975x
Anal. Chem. 2015, 87, 3678−3684

presence of H_2O_2, indicating that the mitochondrial pH was decreased (Figure 6). Then, mitochondrial membrane potential

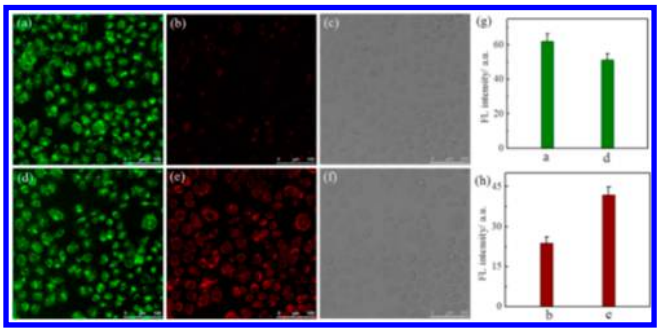

Figure 6. Confocal fluorescence imaging of MCF-7 cells treated with the nanosensor in the absence (a–c) or presence (d–f) of 100 μM H_2O_2. (c, f) Brightfield image. (g, h) Mean fluorescence intensity of nanosensor treated cells in panels a, b, d, and e. The excitation wavelength of a and d is 488 nm. The excitation wavelength of b and e is 633 nm. Scale bars are 100 μm.

($\Delta\psi$) was monitored by rhodamine 123 using CLSM. After incubation with rhodamine 123, a reduced fluorescence signal was observed for H_2O_2 treated cells (Figure S13b) compared with the untreated cells (Figure S13a). It indicated that $\Delta\psi$ was decreased when the cells were treated with H_2O_2. This is because ROS promotes the mitochondrial permeability transition pore opening via oxidation of the matrix glutathione.[33] The decreased $\Delta\psi$ was coincident with the reduction of mitochondrial pH, which was in accordance with the previous report.[15]

Dichloroacetate (DCA) is a small molecule generic drug, which can inhibit mitochondrial pyruvate dehydrogenase kinase and shift metabolism from glycolysis to glucose oxidation. This reverses the suppressed mitochondrial apoptosis in cancer cells but not normal cells.[34] We next examined the availability of the nanosensor for monitoring the changes of H_2O_2 and pH in the human breast cancer cell line (MCF-7) and normal immortalized human mammary epithelial cell line (MCF-10A) by DCA stimulation. When the nanosensor-treated MCF-7 cells were incubated with DCA, a decreased green fluorescence signal (Figure 7b) was observed while the red fluorescence was increased (Figure 7f), indicating that the pH value was decreased and H_2O_2 concentration was increased.

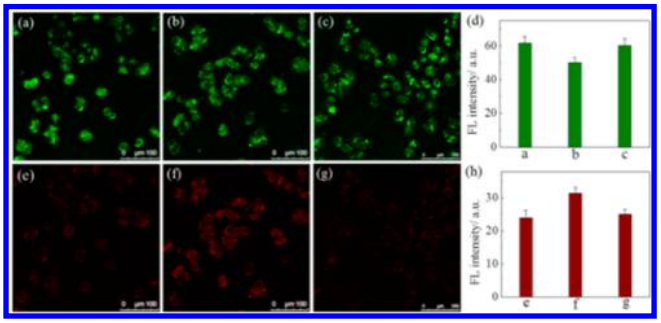

Figure 7. Confocal fluorescence imaging of MCF-7 cells treated with the nanosensor in the absence of DCA (a, e), in the presence of DCA (b, f), and in the presence of DCA and rotenone (c, g). Mean fluorescence intensity of nanosensor treated cells in panels a–c and e–g (d, h). The excitation wavelength of a, b, and c is 488 nm. The excitation wavelength of e, f, and g is 633 nm. Scale bars are 100 μm.

Moreover, a gradually decreased green fluorescence signal (Figure S14A) and increased red fluorescence (Figure S14B) were observed via time-dependent experiments, indicating that the nanosensor is capable of real-time visualization of the H_2O_2 and pH fluctuations in mitochondria. Further experiments showed that $\Delta\psi$ was decreased in MCF-7 cells after DCA stimulation (Figure S7b). The generated mitochondrial H_2O_2 in MCF-7 cells after DCA stimulation could damage the redox sensitive complex I, inhibiting H^+ efflux and decreasing $\Delta\psi$. Thus, the pH of mitochondria is declined. Next, an inhibitor of mitochondrial electron transport, rotenone, was employed to abrogate the DCA-induced effect. The green and red fluorescence signal (Figure 7c,g) remained almost constant in the control due to the inhibiting effect of rotenone. Further study was performed to investigate the ability of the nanosensor to detect the changes in the MCF-10A cells treated with DCA. Figure 8 showed that the green and red fluorescence signal did

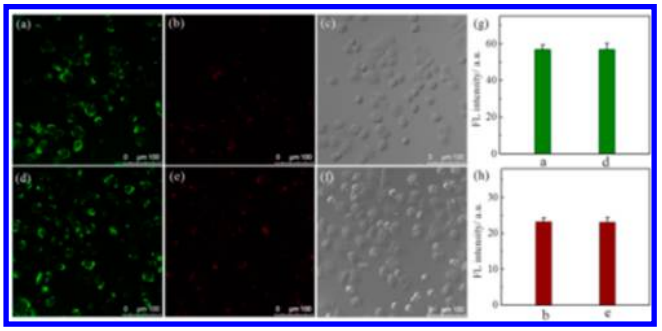

Figure 8. Confocal fluorescence imaging of MCF-10A cells treated with the nanosensor in the absence of DCA (a–c) and in the presence of DCA (d–f). (c, f) Brightfield image. (g, h) Mean fluorescence intensity of nanosensor treated cells in panels a, b, d, and e. The excitation wavelength of a and d is 488 nm. The excitation wavelength of b and e is 633 nm. Scale bars are 100 μm.

not show obvious change in nanosensor-treated MCF-10A cells in the presence of DCA, implying that DCA has no effect on the normal cells. Also, $\Delta\psi$ displayed no obvious changes after MCF-10A cells incubated with DCA (Figure S15d). Moreover, it was observed that the MCF-7 cells (Figure S15a) had significantly more hyperpolarized $\Delta\psi$ compared to MCF-10A cells (Figure S15c). The results are consistent with a previous report.[18] Thus, it demonstrates that the nanosensor is capable of visualizing the H_2O_2 and pH fluctuations in mitochondria, implying that the nanosensor could be as an appealing imaging tool to dissect the interplaying roles and dynamic changes of these biomolecules for comprehending the intracellular reaction mechanism of drugs.

CONCLUSIONS

In summary, we have developed a novel fluorescent nanosensor for real-time monitoring and imaging the fluctuations of mitochondrial H_2O_2 and pH in living cells, which is difficult to achieve by molecular fluorescent probes and green fluorescent protein probes. The nanosensor could simultaneously monitor the changes of H_2O_2 and pH without mutual interference. Fluorescence imaging experiments demonstrate that the nanosensor is capable of reliably reporting and selectively discriminating the H_2O_2 and pH fluctuations in mitochondria at the same time and position with bicolor imaging. The nanosensor has potential utility in disentangling the interplaying roles of mitochondrial H_2O_2 and pH for better

DOI: 10.1021/ac503975x
Anal. Chem. 2015, 87, 3678–3684

understanding of mitochondrial physiology and pathology. More significantly, the proposed strategy should be applicable to construct other sensors for simultaneous sensing and imaging of multiple subcellular analytes in living cells.

■ ASSOCIATED CONTENT

Supporting Information

Experimental details and supporting figures. This material is available free of charge via the Internet at http://pubs.acs.org.

■ AUTHOR INFORMATION

Corresponding Author

*Fax: (86)531 86180017. E-mail: tangb@sdnu.edu.cn.

Author Contributions

†Limin Yang and Na Li contributed equally to this work.

Notes

The authors declare no competing financial interest.

■ ACKNOWLEDGMENTS

This work was supported by 973 Program (2013CB933800) and National Natural Science Foundation of China (21227005, 21390411, 91313302, 21422505, 21375081).

■ REFERENCES

(1) Saraste, M. *Science* **1999**, *283*, 1488−1493.
(2) Gogvadze, V.; Orrenius, S.; Zhivotovsky, B. *Semin. Cancer Biol.* **2009**, *19*, 57−66.
(3) Kroemer, G.; Reed, J. C. *Nat. Med.* **2000**, *6*, 513−519.
(4) Wallace, D. C. *Science* **1999**, *283*, 1482−1488.
(5) Lin, M. T.; Beal, M. F. *Nature* **2006**, *443*, 787−795.
(6) Kroemer, G.; Pouyssegur, J. *Cancer Cell* **2008**, *13*, 472−482.
(7) Galluzzi, L.; Morselli, E.; Kepp, O.; Vitale, I.; Rigoni, A.; Vacchelli, E.; Michaud, M.; Zischka, H.; Castedo, M.; Kroemer, G. *Mol. Aspects Med.* **2010**, *31*, 1−20.
(8) Moreira, P. I.; Santos, M. S.; Oliveira, C. R. *Antioxid. Redox Signal.* **2007**, *9*, 1621−1630.
(9) Finkel, T. *Nat. Rev. Mol. Cell Biol.* **2005**, *6*, 971−976.
(10) Rhee, S. G. *Science* **2006**, *312*, 1882−1883.
(11) Wallace, D. C. *Nat. Rev. Cancer* **2012**, *12*, 685−698.
(12) Belousov, V. V.; Fradkov, A. F.; Lukyanov, K. A.; Staroverov, D. B.; Shakhbazov, K. S.; Terskikh, A. V.; Lukyanov, S. *Nat. Methods* **2006**, *3*, 281−286.
(13) Yin, L.; Stearns, R.; González-Flecha, B. *J. Cell Biochem.* **2005**, *94*, 433−445.
(14) Satoh, T.; Enokido, Y.; Aoshima, H.; Uchiyama, Y.; Hatanaka, H. *J. Neurosci. Res.* **1997**, *50*, 413−420.
(15) Matsuyama, S.; Llopis, J.; Deveraux, Q. L.; Tsien, R. Y.; Reed, J. C. *Nat. Cell Biol.* **2000**, *2*, 318−325.
(16) Indran, I. R.; Tufo, G.; Pervaiz, S.; Brenner, C. *Biochim. Biophys. Acta* **2011**, *1807*, 735−745.
(17) Srikun, D.; Albers, A. E.; Chang, C. J. *Chem. Sci.* **2011**, *2*, 1156−1165.
(18) Bonnet, S.; Archer, S. L.; Allalunis-Turner, J.; Haromy, A.; Beaulieu, C.; Thompson, R.; Lee, C. T.; Lopaschuk, G. D.; Puttagunta, L.; Bonnet, S.; Harry, G.; Hashimoto, K.; Porter, C. J.; Andrade, M. A.; Thebaud, B.; Michelakis, E. D. *Cancer Cell* **2007**, *11*, 37−51.
(19) Dickinson, B. C.; Lin, V. S.; Chang, C. J. *Nat. Protoc.* **2013**, *8*, 1249−1259.
(20) Dickinson, B. C.; Chang, C. J. *J. Am. Chem. Soc.* **2008**, *130*, 9638−9639.
(21) Xu, K.; Qiang, M.; Gao, W.; Su, R.; Li, N.; Gao, Y.; Xie, Y.; Kong, F.; Tang, B. *Chem. Sci.* **2013**, *4*, 1079−1086.
(22) Masanta, G.; Heo, C. H.; Lim, C. S.; Bae, S. K.; Cho, B. R.; Kim, H. M. *Chem. Commun.* **2012**, *48*, 3518−3520.
(23) Lee, M. H.; Park, N.; Yi, C.; Han, J. H.; Hong, J. H.; Kim, K. P.; Kang, D. H.; Sessler, J. L.; Kang, C.; Kim, J. S. *J. Am. Chem. Soc.* **2014**, *136*, 14136−14142.
(24) Tantama, M.; Hung, Y. P.; Yellen, G. *J. Am. Chem. Soc.* **2011**, *133*, 10034−10037.
(25) Li, P.; Xiao, H.; Cheng, Y.; Zhang, W.; Huang, F.; Zhang, W.; Wang, H.; Tang, B. *Chem. Commun.* **2014**, *50*, 7184−7187.
(26) Abad, M. F. C.; Benedetto, G. D.; Magalhães, P. J.; Filippin, L.; Pozzan, T. *J. Biol. Chem.* **2003**, *279*, 11521−11529.
(27) Zhang, Z.; Balogh, D.; Wang, F.; Willner, I. *J. Am. Chem. Soc.* **2013**, *135*, 1934−1940.
(28) Li, N.; Yu, Z.; Pan, W.; Han, Y.; Zhang, T.; Tang, B. *Adv. Funct. Mater.* **2013**, *23*, 2255−2262.
(29) Li, Z.; Barnes, J. C.; Bosoy, A.; Stoddart, J. F.; Zink, J. I. *Chem. Soc. Rev.* **2012**, *41*, 2590−2605.
(30) Kobler, J.; Möller, K.; Bein, T. *ACS Nano* **2008**, *2*, 791−799.
(31) Marrache, S.; Dhar, S. *Proc. Natl. Acad. Sci. U.S.A.* **2012**, *109*, 16288−16293.
(32) Lee, M. H.; Han, J. H.; Lee, J. H.; Park, N.; Kumar, R.; Kang, C.; Kim, J. S. *Angew. Chem., Int. Ed.* **2013**, *52*, 6206−6209.
(33) Lam, M.; Oleinick, N. L.; Nieminen, A. L. *J. Biol. Chem.* **2001**, *276*, 47379−47386.
(34) Michelakis, E. D.; Webster, L.; Mackey, J. R. *Br. J. Cancer* **2008**, *99*, 989−994.

DOI: 10.1021/ac503975x
Anal. Chem. 2015, 87, 3678−3684